

1 **Stratospheric and Mesospheric Data Assimilation: The role of**
2 **middle atmospheric dynamics**

3
4
5 Saroja Polavarapu¹ and Manuel Pulido²

6 ¹Environment Canada, Toronto, Ontario, Canada

7 ²Universidad Nacional del Nordeste, Argentina

8
9 August 5, 2015

10
11
12 A chapter for submission to:

13 Volume 3 of "*Data Assimilation for Atmospheric, Oceanic and Hydrologic Applications.*" The first
14 volume was published in 2009, and the second in 2013. Both volumes were published by the Springer,
15 with 27 chapters each, which were based on papers presented at the Sasaki Symposium on data
16 assimilation (DA) in the AOGS meetings along with some invited papers. Prof. Yoshi Sasaki passed
17 away on Mar. 12, 2015. He was a pioneer in atmospheric data assimilation who introduced and applied
18 the variational methods. We plan to dedicate this book to the late Yoshi Sasaki as a memorial volume.

19

ABSTRACT

20 The middle atmosphere refers to the stratosphere and mesosphere and features dynamics and circulations
21 that are fundamentally different from those of the troposphere. The large-scale meridional circulations in
22 the middle atmosphere operate on seasonal and longer time scales and are largely forced by the breaking
23 of upward propagating waves. The winter stratosphere is dominated by large-scale waves and a polar
24 vortex which confines constituents and which is sometimes punctuated by stratospheric sudden warmings.
25 In contrast, the summer stratosphere is quiescent. Meanwhile, the meridional circulation in the
26 mesosphere is mainly driven by the breaking of a broad spectrum of gravity waves that have propagated
27 upward from the troposphere. These facets of middle atmosphere dynamics have implications for, and
28 pose unique challenges to, data assimilation systems whose models encompass this region of the
29 atmosphere. In this work, we provide an overview of middle atmosphere data assimilation in the context
30 of the dynamics of this region. The purpose is to demonstrate how the dynamics can be used to explain
31 the behavior of data assimilation systems in the middle atmosphere, and also to identify challenges in
32 assimilating measurements from this region of the atmosphere. There are two overarching themes.
33 Firstly, we consider the vertical propagation of information through waves, resolved and parameterized,
34 and background error covariances. Secondly, we delve into the dynamical sources of model errors and
35 techniques for their estimation.

36

37 **1. Introduction**

38 The past decade has seen operational weather forecasting centers raise their model lids to the
39 middle or upper mesosphere. The NASA's Global Modeling and Assimilation Office (GMAO) raised its
40 model lid height to 80 km in January 2004. The European Centre for Medium-Range Weather Forecasts
41 (ECMWF) did the same in February 2006, as did the Met Office in November 2009. The Canadian
42 Meteorological Centre (CMC)'s model lid moved to 0.1 hPa (roughly 65 km) in June 2009 (Charron et al.
43 2012). Given that the primary focus of an operational weather forecasting centre is on producing real
44 time forecasts for the troposphere, the extra computational expense invested in raising the model lid to
45 such heights merits an explanation. There are two main motivating factors for making this change. On
46 the one hand, a precise model representation of the stratosphere is expected to increase predictive skill of
47 extended range (10 days to subseasonal) forecasts (Tripathi et al. 2014, Gerber et al. 2012, Charlton et al.
48 2004, 2005b) but more importantly there is a significant number of nadir satellite observations that are
49 sensitive to the middle atmosphere, Figure 1 shows the normalized weighting functions from the
50 Advanced Microwave Sounding Unit (AMSU)-A instrument. Several channels (12-14) exhibit peak
51 sensitivity to upper stratospheric temperature and many others (6-11) have peak or significant sensitivity
52 to lower or mid stratosphere temperature. In order to assimilate these channels, a model would need a
53 good background forecast up to 0.1 hPa, so its sponge layer should begin above this level. This then
54 implies a model lid in the middle mesosphere. Thus the stratosphere and most of the mesosphere are now
55 part of the weather forecasting domain.

56 Since weather forecast models form the basis of major reanalysis efforts such as ERA-Interim
57 (Dee et al. 2011), JRA-55 (Kobayashi et al. 2015) or MERRA (Rienecker et al. 2011), there are now long
58 time series of analyses of the middle atmosphere which serve the climate community. These reference
59 datasets are widely used for assessing and validating climate models, for understanding measurements

60 and driving chemistry transport models (CTMs). Thus a whole community is inspecting assimilation
61 products in the middle atmosphere, providing feedback on successes and deficiencies. In particular,
62 middle atmosphere dynamicists, climatologists and chemists have noted differences in the various
63 reanalysis products and established an international effort (Stratospheric Processes and their Role in
64 Climate (SPARC) Reanalysis Intercomparison Project or S-RIP) to systematically compare the products
65 and provide guidance to climate scientists as to where and when they are reliable as well as to data
66 assimilators (<http://www.sparc-climate.org/activities/reanalysis/>). The very existence of S-RIP points to
67 the value placed on middle atmosphere analyses by climate scientists.

68 There are yet other reasons for assimilating observations of the middle atmosphere, such as
69 driving models with chemistry to quantify stratospheric ozone loss (Shepherd et al. 2014), assessing
70 changes in the transport of constituents (and the Brewer-Dobson circulation) (Hegglin et al. 2014), and
71 better understanding large-scale dynamic events such as sudden stratospheric warmings and their
72 potential impacts or responses under climate change scenarios. Finally, the stratosphere has a memory
73 that can be exploited for improving the skill of seasonal forecasts (Stockdale et al. 2015, Sigmond et al.
74 2013, Marshall and Scaife 2009, Boer and Hamilton 2008) providing yet another motivation for the
75 assimilation of observations into models capable of depicting the middle atmosphere.

76 Middle atmosphere data assimilation has therefore become increasingly relevant to operational
77 and research atmospheric data assimilation efforts. While the same general techniques of data
78 assimilation are applied to all regions of the atmosphere simultaneously, there are reasons to afford
79 middle atmosphere data assimilation separate consideration. Firstly, the dynamics of the middle
80 atmosphere differ from those of the troposphere and, as will be shown below, this has important
81 implications for understanding the behavior of data assimilation systems. Secondly, the degree to which a
82 forecast model captures these dynamics provides insight into the nature of model errors in this region of
83 the atmosphere. Finally, the observing system targeting this region of the atmosphere poses unique
84 challenges. While radiosondes have formed the backbone of tropospheric assimilation systems (whether

85 directly or through the anchoring of bias correction schemes applied to satellite measurements), they only
86 reach as high as the middle stratosphere, leaving much of the middle atmosphere devoid of in situ
87 measurements. Operational satellites sensing the middle atmosphere are primarily nadir sounders such as
88 AMSU (Advanced Microwave Sounding Unit). Since these instruments are sensitive to broad layers of
89 the atmosphere, the vertical structure of the stratosphere and mesosphere cannot be well resolved.
90 Fortunately, with the routine assimilation of Global Positioning System (GPS) Radio Occultation (RO)
91 measurements, the vertical structure of the lower to mid stratosphere can be better resolved (Cardinali and
92 Healy, 2014; Healy and Thépaut, 2006). However, above 35 km, the data become noisier and only
93 weakly constrain the full state despite effectively constraining the bias of satellite measurements. Thus,
94 the vertical structure of the atmosphere above the mid stratosphere remains difficult to estimate.

95 The goal of this article is to present a subjective overview of middle atmosphere data
96 assimilation, from the perspective of middle atmosphere dynamics but targeted to a data assimilation
97 audience. The intent is not to be exhaustive, but rather, illustrative, while maintaining a focus on
98 identifying particular issues and challenges in the middle atmosphere of coupled troposphere-middle
99 atmosphere data assimilation systems. Constituent assimilation is an enormous topic that is relevant for
100 the middle atmosphere, but one that is not considered here. The distribution of constituents is determined
101 by atmospheric transport and mixing as well as chemical reactions. An overview of transport in the
102 middle atmosphere is provided by Andrews et al. (1987) and Shepherd (2007) while Monge-Sanz et al.
103 (2013) discuss the role of assimilation techniques on constituent transport in the context of chemistry
104 transport models. Recent reviews of chemical data assimilation are provided by Bocquet et al. (2015) and
105 Sandu and Chai (2011).

106 The article is organized as follows. In section 2 a brief overview of middle atmosphere
107 dynamics is provided while in section 3 we look at middle atmosphere data assimilation through the lens
108 of middle atmosphere dynamics. Some additional challenges and issues of middle atmosphere data

109 assimilation not previously mentioned are identified in section 4 and a summary of the chapter is
110 presented in section 5.

111

112 **2. Brief overview of middle atmosphere dynamics**

113 In order to understand how forecasting and assimilation systems respond to perturbations such as
114 analysis increments, it is necessary to introduce a few concepts about middle atmosphere dynamics. A
115 very brief introduction of the dynamic features that have some impact on data assimilation is given here,
116 but more detailed accounts are available in textbooks (e.g. Andrews et al. 1987, Vallis 2006) and articles
117 (e.g. Shepherd 2000, 2002, 2007; McLandress 1998; Smith 2004).

118 The middle atmosphere refers to the stratosphere and mesosphere and extends from roughly 10 to
119 80 km above the Earth's surface. Temperature increases with height in the stratosphere due to the
120 absorption of ultraviolet radiation by ozone and decreases with height in the mesosphere as the ozone
121 concentration drops off. The stratosphere is statically stable and the climatological winds are to a first
122 approximation zonal. If we consider the two-dimensional, steady, geostrophic and hydrostatic equations,
123 in the absence of a momentum source, the atmosphere would be in radiative equilibrium balance with
124 outgoing terrestrial radiation balancing incoming solar radiation. This means a cold dark winter pole and
125 a warm sunlit summer pole. Through thermal wind balance, zonal winds increase with height. However,
126 as shown in **Figure 2a**, radiative-equilibrium temperature calculations yield temperatures near the winter
127 pole (dashed lines) that are far too cold compared to observed values (solid lines), and zonal wind speeds
128 that are much too strong (compare dashed and solid lines in **Figure 2b**). McLandress (1998) added a
129 simple Rayleigh friction term as a forcing term in the zonal momentum equation which is linearly
130 proportional to zonal wind with the proportionality constant increasing with height. The resulting
131 temperatures and zonal wind speeds are closer to observations (compare dotted and solid lines in **Figure**
132 **2**) than the radiative equilibrium solution (dashed lines). The conclusion is that some kind of momentum

133 source/sink is needed to explain the observed zonal mean temperatures and winds, as was first
134 hypothesized by Leovy (1964).

135 The origin of this momentum source/sink is breaking waves, which exert a drag or forcing on the
136 zonal mean flow and drive a mean meridional circulation. In the winter stratosphere, large-scale quasi-
137 stationary Rossby waves forced by topography and land-sea contrasts are able to propagate upward
138 through the stratospheric westerlies where they increase in amplitude as density decreases. Eventually
139 they break, impart their (negative) momentum to the zonal mean flow, exerting a drag on the wintertime
140 westerlies. This creates poleward motion through a Coriolis torque and by continuity, descent (and
141 warming through adiabatic compression) over the winter pole. Thus, large-scale waves drive this
142 thermally-indirect circulation, called the Brewer-Dobson circulation. The Brewer-Dobson circulation is
143 important not only for explaining stratospheric temperature distributions, but also for transporting
144 constituents, as is apparent in the accumulation of ozone over the winter pole in **Figure 3**. The conditions
145 for vertical propagation of quasi-stationary Rossby waves (see Andrews et al. 1987, chapter 4.5 or Vallis
146 2006, chapter 13.3) in the case of a constant wind (U) are that $U > 0$ (eastward) and U remains below a
147 critical value (U_c). Thus, these waves cannot propagate into the stratosphere in summer when zonal
148 winds are easterly. Furthermore, in the winter when they can propagate vertically, large-scale waves
149 (wavenumbers 1 to 3) are favoured because the critical wind speed (U_c) decreases rapidly with increasing
150 wavenumber. Thus the winter stratosphere is dominated by waves having large horizontal scales. Due to
151 the fact that quasi-stationary Rossby waves are unable to propagate in easterly zonal wind, the summer
152 stratosphere is characterized by an absence of these waves and so by temperatures closer to radiative
153 equilibrium.

154 The stratospheric jets also act to filter much smaller-scale waves (i.e., gravity waves) which
155 would otherwise propagate up to the mesosphere. In winter when stratospheric winds are westerly and
156 increasing with height, gravity waves with eastward phase speeds may reach their critical level (where the

157 zonal phase velocity equals the zonal wind) in the stratosphere. This removal or “filtering” of eastward
158 propagating waves at their critical levels leads to predominantly westward propagating gravity waves
159 reaching the mesosphere (assuming a westward-eastward isotropic launch gravity wave spectrum). When
160 those waves break in the mesosphere they deposit westward momentum (Lindzen 1981). Similarly, in the
161 summer hemisphere, easterly winds filter westward propagating gravity waves at their critical levels, so
162 that gravity waves which break in the mesosphere deposit eastward momentum. In the mesosphere, this
163 deceleration of the westerlies in the winter hemisphere and deceleration of the easterlies in the summer
164 hemisphere caused by gravity wave momentum deposition create a poleward motion in the winter
165 hemisphere, but equatorward motion in the summer hemisphere. By continuity, there is descent over the
166 winter pole and ascent over the summer pole. Thus small scale gravity waves are responsible for driving
167 the pole-to-pole Murgatroyd-Singleton circulation in the mesosphere seen in the upper part of **Figure 3**.

168 Since the spectrum of Rossby waves propagating upward in the winter stratosphere is
169 dominated by the largest modes, as synoptic scale waves are filtered in the lower stratosphere,
170 these large-scale waves are expected to be well represented in global numerical models. On the
171 other hand, gravity waves are small-scale waves which propagate almost vertically. Therefore,
172 global numerical models are typically not able to directly represent these waves. In order to
173 incorporate the momentum forcing produced by small-scale gravity waves in global numerical
174 models, the drag exerted by the upward propagation and breaking of small-scale gravity waves
175 on the zonal mean flow is accounted for through “gravity wave drag” parameterizations. These
176 parameterizations are divided in two groups: parameterizations of waves of orographic origin
177 and non-orographic gravity wave drag schemes. The generation characteristics of orographically
178 generated waves are well known and have been shown to have a large impact in the lower
179 stratosphere and in particular on the Brewer-Dobson circulation (Li et al 2008, McLandress and
180 Shepherd 2009). Gravity waves from other sources such as fronts, convection, and geostrophic

181 adjustment are modelled through non-orographic gravity wave parameterizations (e.g. Hines
182 1997, Scinocca 2003) and are expected to have a large impact on the upper stratosphere and the
183 mesosphere.

184

185 **3. Impact of middle atmosphere dynamics on data assimilation**

186 The fact that the middle atmosphere is largely driven by waves propagating up from the
187 troposphere has implications for data assimilation. The fundamental difference in stratospheric dynamics
188 between winter and summer also impacts interpretation of data assimilation results and inputs (such as
189 background error covariances). Finally, the importance of gravity waves (that are generated in the
190 troposphere and propagate upward) to the mesospheric circulation means that these signals (which are
191 frequently treated as noise in the troposphere) might need to be better simulated or estimated in the
192 troposphere and lower stratosphere. In this section, we explore how middle atmosphere dynamics impact
193 the inputs and results of data assimilation systems.

194 **3.1. Upward propagation of information**

195 *3.1.1. Propagation of information and errors through resolved waves*

196 **Figure 4** shows averaged analyzed temperature vertical profiles (over the global domain) from a
197 set of data assimilation experiments using a 3D-variational (3D-Var) system for which only the strength
198 of an externally applied filter is varied. As a result of changing the strength of the filter, a large impact on
199 mesospheric temperatures is found. Specifically, the stronger the filter, the colder the global mean
200 mesopause temperature. A difference of 20 K at 90 km is seen between experiments. These results were
201 surprising because the Canadian Middle Atmosphere Model (CMAM) (Scinocca et al. 2008) which was
202 employed in the data assimilation system extends to about 95 km but the observations were inserted only
203 below about 45 km. Thus the filter was targeting imbalance arising from increments below 45 km. Yet

204 below 45 km, the temperature profile averaged over all coincident measurement locations was virtually
205 identical regardless of which filter was employed. This is because the averaging over all profiles smooths
206 whatever degree of noise is present in the profiles obtained with different filters. However, the waves
207 defined by the increments in the troposphere (whether real or spurious) propagate up to the mesosphere
208 where they break and create a drag (momentum forcing) which impacts the zonal mean flow. If they do
209 not break by 80 km they encounter the model sponge layer which is designed to absorb such waves thus
210 preventing their reflection from the model lid at 95 km. The sponge layer is a numerical device acting on
211 departures from the zonal mean flow (Shepherd et al. 1996) that is intended to mimic the fact that in the
212 absence of the model lid these waves would reach higher altitudes where they would break, deposit
213 momentum and create turbulent dissipation generating heating. Eventually the radiation to space balances
214 the wave-generated heating resulting in the temperature profiles seen in **Figure 4**. Thus although the
215 heating is artificially created here through the enforced dissipation of these upward propagating waves,
216 the same process would occur in the real atmosphere though at higher altitudes because of molecular
217 viscosity. Indeed Lübken et al. (2002) show that gravity waves are an important source of heating in the
218 mesopause region. Thus, in **Figure 4**, a stronger, more dissipative filter results in smaller wave
219 momentum flux reaching the mesosphere and less enforced wave breaking and resultant heating in the
220 sponge layer. This hypothesis was confirmed by comparing the temperature variance of time series of
221 analyses from the various experiments (Sankey et al. 2007). The stronger the filter, the smaller the
222 variance. Thus resolved waves in the troposphere and stratosphere can propagate up to the mesosphere
223 and impact the zonal mean or even the global mean flow. The implication is that tropospheric tuning of
224 data assimilation systems can have large impacts on mesospheric analyses. On the other hand, the
225 sensitivity of the mesosphere can also be used to tune assimilation parameters (such as filter strength, as
226 was done in Sankey et al. 2007).

227 Nezlin et al. (2009) demonstrated that even without observations above 45 km, the large scale
228 dynamics (up to wavenumber 10) in the mesosphere could be improved. They also showed that the

229 quality of mesospheric analyses was sensitive to the accuracy of observations taken below 45 km. Both
230 of these facts attest to the vertical propagation of information. (Here we use the term "information" to
231 describe that part of the true atmospheric signal that a given model can resolve.) The observations
232 constrain the atmospheric signal at a given height, and then the dynamics of the model propagates this
233 observational information upward producing an impact at heights where no observations had been
234 assimilated. Since the middle atmosphere is largely forced by upward propagating waves, both
235 information and errors propagate vertically through waves in data assimilation systems. While Nezlin et
236 al. (2009) demonstrated that the vertical propagation of information in a 3D-Var system (the CMAM-
237 Data Assimilation System (DAS)) is theoretically possible through the use of simulated observations, Xu
238 et al. (2011a,b) demonstrated that CMAM-DAS mesospheric winds do indeed compare well to
239 independent measurements on long time scales. This confirms that vertical propagation of information
240 from the troposphere to the mesosphere actually occurs in assimilation systems since no observations in
241 the mesosphere had been assimilated. The same effect is seen in the intraseasonal variability of
242 mesospheric zonal-mean temperature and constituents (carbon monoxide) in a set-up where the CMAM is
243 nudged towards the ERA-Interim reanalysis in the troposphere and stratosphere, and the model is seen to
244 agree well with MLS (Microwave Limb Sounder) observations in the mesosphere (McLandress et al.
245 2013).

246 Even without mesospheric observations, the migrating diurnal and semi-diurnal tidal signals in
247 the mesosphere can be captured (Sankey et al. 2007, Wang et al. 2011, Xu et al. 2011a,b, Hoppel et al.
248 2013). Since these signals are generated by the absorption of solar radiation by water vapour in the
249 troposphere and by ozone in the stratosphere, observations from the troposphere and stratosphere
250 constrain these signals well. Thus agreement of a model's mesospheric tidal amplitudes with
251 observations indicates that the vertical propagation of the signal into the mesosphere is at least partially

252 captured by the model. Of course, assimilation of mesospheric observations, greatly improves agreement
253 with observations (Hoppel et al. 2013).

254 3.1.2. *Propagation of information through background error covariances*

255 The two orders of magnitude increase with height in forecast error variance seen in the bottom
256 left panel of **Figure 5** largely reflects the increasing amplitude of gravity waves from the stratosphere to
257 the mesosphere. As a result, spurious increments in the mesosphere can be produced (top left panel)
258 when the large forecast error variances are combined with small but nonzero correlations in the wings of
259 the weighting function. For example, the analysis increment at 0.01 hPa in the top left panel of **Figure 5**
260 appears at a height where the weighting function for an observation at 10 hPa is virtually zero (i.e. the
261 wings of the weighting function) (top right panel) because the correlation function (bottom right panel,
262 black curve) is not exactly zero at 0.01 hPa. Setting such tiny correlations (which are due to statistical
263 noise) to exactly zero removes much of the spurious mesospheric analysis increments (dashed lines in top
264 left panel). In fact, removing such spurious increments in the mesosphere is imperative when an
265 assimilation system assimilates no mesospheric observations and is therefore unable to damp such errors.
266 In the mesosphere, such spurious increments may be persistent (because of the presence of model and/or
267 observation biases) and can actually lead to physically nonsensical results after only a few weeks of
268 assimilation. Thus information propagated to the mesosphere through background error covariances is
269 not necessarily desirable. Similarly, erroneous small scale vertical structures in background error
270 covariances cannot be damped by measurements if the observing system is lacking in detailed vertical
271 information. This is the case in the upper stratosphere where nadir temperature sounders are the dominant
272 source of information.

273 Since observations of the middle atmosphere are predominantly from satellite-based radiance
274 measurements, the problem of vertical localization of covariances needed for some ensemble-based data
275 assimilation techniques in radiance space is worth noting. The issue is that these types of measurements
276 are related to model quantities integrated in space so that the concept of localization is unclear. Yet the

277 localization of error covariances is important for practical application of ensemble Kalman filters to
278 comprehensive and complex meteorological models. Such localization is frequently done in observation
279 space for computational expediency. The problem identified by Campbell et al. (2010) is that location
280 and distance are ill defined quantities in radiance space so that observation-space localization applied to
281 the usual case of channels with overlapping sensitivities cannot achieve the correct Kalman gain even
282 when observations are known to be perfect. Ideally, the vertical localization must therefore be at least as
283 broad as the weighting functions but not so broad that the suppression of spurious correlations due to
284 sampling errors become ineffective. On the other hand, localization in model space does not suffer from
285 this problem.

286 3.1.3. *Propagation of information through gravity wave drag schemes*

287 Gravity wave drag (GWD) schemes can also propagate information from the troposphere and
288 stratosphere to the mesosphere. GWD schemes parameterize (represent simplifications of) the processes
289 of gravity wave generation in the troposphere, vertical propagation and nonlinear saturation. The output
290 of such a scheme is a drag or forcing term for the momentum equations. GWD schemes are needed in
291 climate models because their coarse horizontal resolutions lead to insufficient forcing of the meridional
292 circulation and insufficient downwelling (and warming) over the winter pole (as well as insufficient
293 upwelling and cooling over the summer pole). Thus, without a GWD scheme, climate models can suffer
294 from the “cold pole” problem, which is particularly evident in the southern hemisphere where there are
295 fewer forced planetary waves (Austin et al., 2003).

296 GWD schemes can also vertically propagate information in data assimilation systems (Ren et al.
297 2008). Observations are used to define winds in the troposphere and stratosphere which filter resolved
298 gravity waves which might otherwise reach the mesosphere. Similarly, the parameterized impact of
299 subgrid scale gravity waves in GWD schemes produce a force on the mesospheric flow (McLandress et
300 al. 2013). The benefit of a GWD scheme on mesospheric analyses was demonstrated by Ren et al.

301 (2011). Background or 6-h forecasts were closer to independent observations of mesospheric temperature
302 (from SABER retrievals) when a GWD scheme was used (**Figure 6**). The benefit was quite large if no
303 mesospheric observations were assimilated, but still apparent even if they were assimilated. Since
304 mesospheric analyses obtained with a model using a GWD scheme but with no mesospheric observations
305 were close to independent measurements, it is evident that GWD is able to propagate useful information
306 to the mesosphere. At ECMWF, the same GWD scheme used in Ren et al. (2011) was implemented
307 operationally, and shown to improve the bias in temperature at the stratopause at the winter pole in 5-day
308 forecasts (Orr et al., 2010).

309

310 **3.2. Understanding forecast improvements**

311 The winter polar stratosphere is dominated by westerly winds that increase with height and define
312 a polar vortex (polar night jet). In the Northern Hemisphere, this vortex is occasionally disrupted by
313 stratospheric sudden warming (SSW) events during which temperatures can rise dramatically (by 50 K in
314 one week). Simultaneously, the climatological westerly winds weaken and may even become easterly.
315 Mesospheric coolings can also occur in conjunction with stratospheric warmings. Since SSW events are
316 primarily driven by planetary waves propagating up from the troposphere, such events involve vertical
317 coupling from the troposphere to the mesosphere. Baldwin and Dunkerton (2001) showed that the
318 dominant mode of slowly varying wintertime variability called the Northern Annular Mode (or NAM) has
319 a spatial structure which is similar from the surface to over 50 km altitude, thus indicating a coupling of
320 the troposphere and stratosphere. (At the surface the pattern is sometimes called the Arctic Oscillation.)
321 The NAM pattern at 10 hPa is a disk of similarly signed values around the pole with oppositely signed
322 values in a ring or annulus around this. A projection of the geopotential height onto this pattern indicates
323 the relative strength of the polar vortex. A strongly positive projection indicates a stronger than normal
324 polar vortex, while a strongly negative projection indicates a weaker than normal vortex. Moreover,
325 when time series of strongly positive or negative NAM events are composited, the vertical coupling

326 becomes apparent. Specifically, a large stratospheric event, such as an SSW, will appear in the mid-
327 stratosphere (10 hPa is often used as a reference level) about ten days prior to its appearance at the
328 surface. Once the NAM signal appears in the troposphere (300 hPa), the same sign of the NAM index
329 persists in the troposphere for around 60 days. During this time, the troposphere is characterized by a
330 particular climatology. For instance, during a strong vortex event, cool winds would flow over eastern
331 Canada, North Atlantic storms would bring rain and mild temperatures to northern Europe and drought
332 conditions would prevail in the Mediterranean (Thompson and Wallace 2001). Thus, the stratospheric
333 modulation of tropospheric climate suggests a predictive skill which can be exploited on the week to
334 seasonal timescales (e.g. Douville 2009). Charlton et al. (2004, 2005b) also showed that stratospheric
335 initial conditions can impact tropospheric forecast skill on the 10-15 day timescale. Various mechanisms
336 have been proposed to explain the stratospheric modulation of tropospheric climate on the week to
337 seasonal timescale but there is no consensus yet as to which is the most important one (Charlton et al.
338 2005a, Tripathi et al. 2014).

339 On shorter (medium range weather forecasting) time scales, middle atmosphere dynamics are still
340 useful for understanding forecast improvements. When the Canadian Meteorological Centre raised the lid
341 of its operational forecast model from 10 to 0.1 hPa, most (over 80%) of the improvement in forecast
342 skill (of both stratosphere and troposphere) was achieved without new measurements in the upper
343 stratosphere (AMSU-A ch. 11-14 and GPS RO between 30-40 km) (Charron et al. 2012). This means
344 that an improved modeling of the stratosphere is sufficient to obtain improved upper stratospheric
345 analysis (where no new data were assimilated). Moreover, the improvement was greatest in the winter for
346 both hemispheres. Thus improvement depended more on season (when the stratosphere was dynamically
347 active) than on hemisphere (or observation distribution). Furthermore, when additional observations in
348 the upper stratosphere were assimilated, they were beneficial in winter but not in summer. These results
349 are understandable in the context of middle atmosphere dynamics. Just as tropospheric observations are

350 most useful when dynamic activity (such as baroclinic wave development) is occurring, stratospheric
351 observations are most beneficial when the stratosphere is dynamically active (in winter).

352 Because of the prevalence of gravity waves and divergent motions in the mesosphere (Koshyk et
353 al. 1999), and the unlikelihood of sparse observations being able to resolve these waves, it is not obvious
354 how beneficial the assimilation of mesospheric observations will be. By comparing forecasts started from
355 analyses in the middle atmosphere (100-0.1 hPa) with those started from climatology in the middle
356 atmosphere, Hoppel et al. (2008) found that the assimilation of middle atmospheric observations were
357 beneficial for winter high latitudes up to the 10-day forecast lead time. In the summer, when the
358 stratosphere is quiescent and dominated by zonal mean flow, persistence or climatology works reasonably
359 well so the benefit of assimilation is not as apparent. On the other hand, mesospheric observations also
360 help to improve the depiction and forecasts of certain planetary waves in the mesosphere as well as
361 reducing biases in zonal mean fields stemming from model errors (Hoppel et al. 2013).

362

363 **3.3. Model error**

364 *3.3.1. Bias estimation*

365 Since not all the resolved waves will be correctly analysed because the observing system can
366 detect only certain spatial scales, and some of the resolved waves are forced in the models by
367 parameterization schemes which are imperfect (e.g. deep convection), we should expect errors in the
368 meridional circulation. Errors in the forcing of a meridional circulation should then lead to latitudinally
369 varying biases. Thus, we should expect bias in zonal mean fields in stratospheric forecasts. Observations
370 (such as those from nadir sounders) also have biases and require a pre-assimilation bias-correction
371 procedure, so the challenge is to separate these two sources of biases. Moreover, observation bias
372 correction schemes often rely on an assumption of unbiased forecasts—which is clearly invalid in the
373 stratosphere. Dee and Uppala (2009) noted that improvement in the stratospheric bias of ERA-interim
374 over ERA-40 was achieved through the introduction of variational bias correction (Derber and Wu 1998).

375 In this procedure, bias correction parameters are added to the control vector so that all observations—
376 including those which are not corrected, such as radiosondes—are used to determine their values. This
377 then forces a consistency among observations which are being bias corrected (e.g. the same instrument on
378 different platforms). Of course, even with variational bias correction, the bias so-determined could be due
379 to either a bias in observations or observation operators or to a bias in the model forecast. Since the bias
380 correction is applied to the observation, only the former type of bias is desired. Thus care must be taken
381 to ensure that the recovered bias is truly due to the observations. To some extent, the anchoring of the
382 assimilation system by uncorrected observations (such as radiosondes) reduces the likelihood that model
383 bias will be detected. However, in the upper stratosphere and mesosphere where few uncorrected
384 observations exist, the danger of correcting for model bias is considerable. Thus Dee and Uppala (2009)
385 chose to leave the top peaking channel (SSU channel 3 or AMSU-A channel 14) uncorrected in the ERA-
386 interim, in order to anchor the system. This resulted in a reduced warm bias near the model top. Since a
387 warm bias had independently been attributed to the model forecast (McNally 2004) the results were
388 positive. So although variational bias correction has proven to be a valuable tool for reanalyses as well as
389 operational assimilation systems, the problem of separating model and measurement bias in the upper
390 stratosphere or mesosphere remains (Hoppel et al. 2013). Leaving a certain instrument uncorrected still
391 creates difficulty when it is present on multiple platforms, or when the observing system changes (e.g.
392 when the top peaking channel changed from SSU ch. 3 to AMSU-A ch. 14). Furthermore, whatever bias
393 exists in the uncorrected measurement will appear in the analyses. Several distinct temporal
394 inhomogeneities in global-mean ERA-Interim temperatures were identified by McLandress et al. (2014).

395 3.3.2. *Unresolved gravity wave drag estimation*

396 The breaking of small-scale gravity waves in the upper stratosphere and mesosphere plays an
397 important role in driving the meridional circulation and thus the impact of these small-scale waves can be
398 detected in large-scale observations such as nadir or AMSU-A satellite measurements. Therefore, the

399 systematic biases found in the model compared to observations may be associated to a large extent with
400 those small-scale gravity wave breaking processes that are not resolved in the model but have a large
401 global impact. Data assimilation techniques which are used to produce analyses can also be used to help
402 diagnose systematic model error. For example, McLandress et al (2012) used the time averaged zonal
403 mean zonal wind analysis increments to identify missing gravity wave drag in the southern hemisphere
404 while Pulido (2014) employed systematic differences of potential vorticity between analyses and
405 forecasts to determine momentum forcing via potential vorticity inversion. In addition, data assimilation
406 techniques can also be used to estimate the missing momentum forcing in the model as a product of the
407 assimilation. Since this missing forcing may be associated to a large extent with gravity wave drag due to
408 unresolved waves, this information can then be used to constrain gravity wave drag parameterization
409 schemes. For example, Pulido and Thuburn (2005) applied a 4D variational assimilation (4D-Var)
410 technique to estimate the missing momentum forcing in the model instead of estimating an initial state.
411 The optimal momentum forcing is the one whose model state evolution is associated with the minimum
412 of the cost function.

413 One helpful aspect of middle atmosphere data assimilation is that the only two processes that are
414 parameterized in models at that height range are radiation and the dissipation of small-scale gravity
415 waves. Since the physics of radiation is well known and only has a large impact on long (seasonal) time
416 scales, the missing zonal momentum forcing at these heights on shorter time scales may be mainly
417 attributed to small-scale gravity waves (Pulido and Thuburn 2006). The optimal momentum forcing
418 estimated with 4D-Var resembles that expected from the filtering of an isotropic gravity wave spectrum
419 (Lindzen, 1981), with large deceleration centres at high latitudes during the winter and summer (Pulido
420 and Thuburn, 2008). On the other hand, it is less evident that the estimated forcing at high latitudes during
421 equinox is associated with an isotropic gravity wave spectrum.

422 3.3.3. *Parameter estimation*

423 Models have a large number of parameters that are not directly observable. Currently, climate
424 modelers infer the values of such unknown parameters manually by comparing the climatology of model
425 integrations with the observed climatology. These inferred parameters may then change if resolution,
426 parameterizations or other parameter values are changed in the model. Data assimilation provides an
427 objective approach to the estimation of unknown model parameters (Ruiz et al 2013). Online parameter
428 estimation techniques based on the ensemble Kalman filter or 4DVar usually define an augmented state
429 which is composed of the model state and also the parameters to be estimated. However, the parameters
430 are not directly constrained by observations as is the model state. Instead, the parameters are constrained
431 through background error correlations between the parameters and model state variables.

432 Gravity wave drag parameters related to the launch wave spectrum and to the saturation and
433 breaking properties of the waves (which determine the gravity wave drag vertical profile) are poorly
434 known from observations. Various techniques have been employed to estimate reasonable values for such
435 parameters. Watanabe (2008) used the results of a high resolution global simulation to determine the
436 characteristics of wave momentum fluxes and to estimate the launch wave spectrum parameters in the
437 Hines parameterization scheme. Some efforts have also been devoted to using high resolution satellite
438 observations (e.g. Atmospheric InfraRed Sounder or AIRS, High Resolution Dynamics Limb Sounder or
439 HIRDLS) to constrain the launch gravity wave spectrum (Alexander et al. 2010). In addition, inverse
440 techniques based on data assimilation have been used to estimate gravity wave parameters. Pulido et al.
441 (2012) proposed an offline data assimilation technique based on a genetic algorithm that uses the
442 estimated missing momentum forcing to constrain launch momentum flux and saturation parameters.
443 Tandeo et al (2015) proposed an ensemble Kalman filter (EnKF) coupled to an expectation maximization
444 algorithm to estimate parameters from an orographic gravity wave drag scheme and also to estimate
445 initial background error covariances which are essential for convergence of the filter in a perfect model
446 experiment. They show that in the presence of model error the filter may converge to different optimal

447 parameters depending on the choice of the first guess value. In general, the estimation of parameters using
448 data assimilation techniques faces a number of unique challenges which require further development or
449 refinement. These challenges are associated with the highly nonlinear nature of the model state response
450 to parameters changes in the context of current assimilation techniques (EnKF and 4DVar) which are
451 based on the linear-Gaussian assumption. To deal with this limitation, some potential solutions have been
452 proposed such as the combination of an offline genetic algorithm with a 4DVar technique (Pulido et al
453 2012), the use of a hybrid EnKF-particle filter, with EnKF for the state variables and a particle filter
454 applied to the parameters (Santitissadeekorn and Jones 2015) and the afore-mentioned EnKF combined
455 with an Expectation-Maximization algorithm (Tandeo et al 2015). A second major challenge is parameter
456 estimation in the presence of model error. In this regard, a recent study found a positive impact
457 particularly when parameter estimation was combined with model error treatment approaches (Ruiz and
458 Pulido, 2015). A third challenge is the interaction between different parameterizations. While this issue is
459 particularly important for tropospheric data assimilation (e.g. interactions between a planetary boundary
460 layer scheme and a convective scheme), it is not as relevant for middle atmosphere data assimilation, as
461 noted earlier.

462

463 **4. Challenges in middle atmosphere data assimilation**

464 While in section 3, we have already noted some challenges in middle atmosphere data
465 assimilation in the context of the topics discussed earlier, in this section we focus on issues that have not
466 yet been raised or fully considered.

467 A characteristic of the observing system for the middle atmosphere is the difficulty of obtaining
468 in situ measurements apart from radiosondes and aircraft observations. Thus, as noted earlier, the vertical
469 structure above the lower stratosphere is not well observed from operational satellites since nadir
470 sounders are sensitive to temperatures over thick layers. On the other hand, GPS radio occultation
471 measurements have been very beneficial not only for their information content and vertical resolution

472 (e.g. Cardinali and Healy, 2014; Healy and Thépaut, 2006) but also for their very low bias which allows
473 them to serve as anchors in bias correction schemes for satellite observations (Cucurull et al, 2014). The
474 constraint of GPS RO data on analyses, however, diminishes as the data become noisier in the upper
475 stratosphere, even as their effectiveness for anchoring the bias correction of satellite data extends
476 throughout the stratosphere (e.g. Cucurull et al. 2014, Charron et al. 2012). Limb sounders such as
477 MIPAS (Michelson Interferometer for Passive Atmospheric Sounding) on Envisat (Environmental
478 satellite), Atmospheric Chemistry Experiment (ACE) aboard SciSat, Microwave Limb Sounder (MLS)
479 on EOS AURA and Sounding of the Atmosphere Using Broadband Emission Radiometry (SABER)
480 aboard TIMED also provide (or did provide) useful information on vertical structure, but these
481 instruments have been on research not operational satellites. As a result, these observations are useful for
482 reanalyses and non-operational assimilation systems but not in operational systems unless they are
483 available in real time (as in the case of MIPAS). Moreover, concern has been expressed over the lack of
484 plans for new limb sounders in the future (Errerra et al., 2015). In the tropics where simple dynamical
485 balances between mass and wind fields are lacking, wind observations are vital but sparse. The
486 Atmospheric Dynamics Mission (ADM-Aeolus) will measure winds globally up to 30 km using an active
487 sensor which will help to better constrain the tropical lower stratosphere but in the mesosphere where
488 unbalanced motions are important, the absence of wind measurements remains an issue. Furthermore,
489 ADM-Aeolus will only measure line-of-sight winds, not vector winds, so a reasonable first guess is
490 required in order to use the information. The only real time observations of the mesosphere are from the
491 SSMIS instrument, however Hoppel et al. (2013) note that apart from the F19 and F20 deployments of the
492 Defense Meteorological Satellite Program (DMSP), there are no other plans for upper atmospheric
493 sounding channels on other satellite sensors raising the possibility of an unconstrained mesosphere
494 analysis in the future. Given that the mesosphere provides the upper boundary for the stratosphere,
495 negative impact on the quality of meteorological forecasts from a paucity of mesospheric measurements is
496 plausible.

497 The usual filtering of or the imposition of balance constraints on the initial state in the data
498 assimilation cycle (Daley 1991) to eliminate gravity waves should be avoided to keep relevant
499 information for the middle atmosphere. On the other hand, most data assimilation techniques which are
500 intermittent (e.g. EnKF, 3DVar) produce temporal discontinuities in the state variables when observations
501 are assimilated, therefore the generation of spurious gravity waves is inevitable with these techniques
502 (e.g. Sankey et al., 2007). A promising way to avoid this issue is the use of an incremental analysis update
503 (IAU) approach (Bloom et al., 1996) or nudging techniques (Lei et al., 2012). The idea behind these
504 approaches is to distribute the forcing toward observations along the whole assimilation window, in the
505 first case through a uniform forcing term (i.e. the analysis increment), or in the second case through a
506 linear damping forcing term (nudging term) that pushes the model toward the analyses. These approaches
507 give a smooth evolution of the model state so that they avoid the spurious generation of gravity waves
508 due to spin-up processes and in turn avoid the need to apply external filters. The smooth model state
509 evolution then permits cleaner momentum budget studies. The use of IAU was also found helpful for
510 capturing mesospheric tides (Sankey et al. 2007, Wang et al. 2011). Since the migrating diurnal tide is
511 already captured by general circulation models, its signal in the mesosphere can also be captured even
512 without mesospheric observations, if care is taken when filtering analysis increments. The incremental
513 analysis update approach was employed in combination with 3D variational assimilation to produce
514 Modern-Era Retrospective Analysis for Research and Applications (MERRA) reanalyses by the NASA-
515 GEOS data assimilation system (Rienecker et al 2011). A 4D extension of the IAU procedure was
516 developed by Lorenc et al. (2015) and is used in the hybrid ensemble variational assimilation scheme
517 which is used for deterministic medium range weather forecasts at Environment Canada (Buehner et al.
518 2015).

519 Section 3.1 highlighted the fact that information propagates vertically with resolved and
520 unresolved waves, but it is worth remarking that by the same mechanisms, errors can also propagate
521 vertically. For example, Nezlin et al. (2009) show that increasing the observation error applied to

522 simulated tropospheric observations deteriorates the quality of stratospheric and mesospheric analyses.
523 Thus the tuning of assimilation schemes for tropospheric forecast quality may have unintended impacts
524 on the analyses of the middle atmosphere (e.g. Sankey et al. 2007). On the other hand, the upscale
525 propagation of errors and concomitant loss of predictability characteristic of the troposphere is not as
526 severe in the middle atmosphere (Ngan and Eperon, 2012). Moreover, increased resolution and better
527 resolved gravity waves may actually help to improve predictability on longer time scales. This may
528 sound counter intuitive given the flat kinetic energy spectrum in the mesosphere due to large amplitude
529 gravity waves (Koshyk et al. 1999), but the hypothesis of Ngan and Eperon (2012) is that predictability
530 can be increased if the gravity waves are better resolved because the upscale error cascade is slower for
531 these waves than for balanced modes. Whether the results of this theoretical study are borne out in
532 operational data assimilation systems is yet to be determined.

533 The impact of the stratosphere on tropospheric forecasts has primarily been associated with
534 certain “extreme” dynamical events in the stratosphere such as sudden warmings. However, there remain
535 many questions associated with the stratospheric influence on tropospheric forecasts, such as whether the
536 influence extends beyond such extreme events and how far in advance extreme events can be predicted.
537 These are some of the questions that are being addressed by a new international collaboration within
538 SPARC called the Stratospheric Network on Assessment of Predictability (SNAP, [http://www.sparc-](http://www.sparc-climate.org/activities/assessing-predictability/)
539 [climate.org/activities/assessing-predictability/](http://www.sparc-climate.org/activities/assessing-predictability/)). Operational weather centers have seen improvements in
540 tropospheric forecasts when raising their model lids (e.g. Charron et al. 2012), however such changes are
541 made simultaneously with other assimilation system changes. Thus another goal of SNAP is to try to
542 isolate the extent to which accurate stratospheric forecasts contribute to tropospheric predictability.

543 **5. Summary**

544 Information can be propagated vertically in data assimilation systems through covariances,
545 vertically propagating waves, and gravity wave drag schemes. As a result, very large scales in the

546 mesosphere can be improved even without assimilating any mesospheric measurements. The fact that the
547 middle atmosphere is driven by vertically propagating waves has important implications for data
548 assimilation systems. (1) Tropospheric waves (whether correctly simulated or not) impact zonal mean
549 fields in the stratosphere and mesosphere. This means that apparently random signals (e.g. waves) can
550 produce nonlocal systematic errors (e.g. a zonal mean bias). (2) Since not all waves are correctly
551 simulated, and the large wavenumber part of the spectrum is not resolved, we should expect bias (errors
552 in zonal mean) in the mesosphere and stratosphere. This has implications for observation bias correction
553 schemes that assume the background forecast is unbiased. (3) Mesospheric analyses are sensitive to
554 errors in tropospheric analyses. On the other hand, perhaps we can use this sensitivity to help choose
555 assimilation parameters in the troposphere. (4) Information propagates up (through resolved waves during
556 the forecast step). Some of the large scales in the mesosphere can be improved even with no mesospheric
557 observations if tropospheric wave forcing is captured and the middle atmosphere is well modelled. The
558 assimilation of observations will additionally improve mesospheric analyses on large scales thus
559 providing a better upper boundary condition with which to constrain forecasts of the troposphere and
560 lower stratosphere, particularly on longer time scales.

561 Given the fact that the middle atmosphere is largely driven by vertically propagating waves
562 including gravity waves, and the fact that global climate models often have coarse resolution, it is
563 necessary to parameterize the impact of the dissipation of subgrid scale waves on the zonal mean flow
564 thus introducing a potential source of model error. Data assimilation is useful for estimating the missing
565 drag attributed to such waves as well as for estimating parameters involved in gravity wave drag schemes.

566 **6. Acknowledgements**

567 We are grateful to Ted Shepherd, Josep Aparicio and Martin Charron for providing helpful
568 comments on an earlier version of this article. The work involving the CMAM-DAS was supported by
569 the C-SPARC project which was funded by the Canadian Foundation for Climate and Atmospheric

570 Sciences (CFCAS) and the Canadian Space Agency (CSA). MP's work was partially funded by a
571 CONICET Grant PIP 112-20120100414CO.

572

573 **7. References**

574 Alexander, M. J., M. Geller, C. McLandress, S. Polavarapu, P. Preusse, F. Sassi, K. Sato, S. Eckermann,
575 M. Ern, A. Hertzog, Y. Kawatani, M. Pulido, T. Shaw, M. Sigmond, R. Vincent, S. Watanabe, 2010:
576 Recent Developments in Gravity Wave Effects in Climate Models, and the Global Distribution of Gravity
577 Wave Momentum Flux from Observations and Models. *Q. J. Roy. Meteorol. Soc.*, **136**, 1103–1124.

578

579 Andrews, D. G., J. R. Holton and C. B. Leovy, 1987: *Middle Atmosphere Dynamics*. Academic Press.
580 489 pp.

581

582 Austin, J., D. Shindell, S. R. Beagley, C. Bruhl, M. Dameris, E. Manzini, T. Nagashima, P. Newman, S.
583 Pawson, G. Pitari, E. Rosanov, C. Schnadt, and T. G. Shepherd, 2003: Uncertainties and assessments of
584 chemistry-climate models of the stratosphere. *Atmos. Chem. Phys.* **3**, 1-27.

585

586 Baldwin, M. P. and T. J. Dunkerton, 2001: Stratospheric Harbingers of anomalous weather regimes.
587 *Science*, **294**, 581 – 584, DOI: 10.1126/science.1063315.

588

589 Bloom, S. C., Takacs, L. L., Da Silva, A. M., Ledvina, D., 1996: Data assimilation using incremental
590 analysis updates. *Mon. Wea. Rev.*, **124**, 1256-1271.

591

592 Bocquet, M., Elbern, H., Eskes, H., Hirtl, M., Žabkar, R., Carmichael, G. R., Flemming, J., Inness, A.,
593 Pagowski, M., Pérez Camaño, J. L., Saide, P. E., San Jose, R., Sofiev, M., Vira, J., Baklanov, A.,

594 Carnevale, C., Grell, G., and Seigneur, C.: Data assimilation in atmospheric chemistry models: current
595 status and future prospects for coupled chemistry meteorology models, *Atmos. Chem. Phys.*, **15**, 5325-
596 5358, doi:10.5194/acp-15-5325-2015, 2015.

597

598 Boer, G. J. and K. Hamilton, 2008: QBO influence on extratropical predictive skill. *Clim. Dyn.* **31**:987-
599 1000.

600

601 Buehner, M., R. McTaggart-Cowan, A. Beaulne, C. Charette, L. Garand, S. Heilliette, E. Lapalme, S.
602 Laroche, S. R. Macpherson, J. Morneau, and A. Zadra, 2015: Implementation of Deterministic Weather
603 Forecasting Systems Based on Ensemble–Variational Data Assimilation at Environment Canada. Part I:
604 The Global System. *Mon. Wea. Rev.*, **143**, 2532–2559.

605

606 Campbell, W. F., C. H. Bishop and D. Hodyss, 2010: Vertical covariance localization for satellite
607 radiances in Ensemble Kalman Filters. *Mon. Wea. Rev.*, **138**, 282-290. DOI: 10.1175/2009MWR3017.1

608

609 Cardinali, C. and S. Healy, 2014: Impact of GPS radio occultation measurements in the ECMWF
610 system using adjoint-based diagnostics. *Q. J. R. Meteorol. Soc.* **140**: 2315–2320, DOI:10.1002/qj.2300

611

612 Charlton, A. J., A. O’Neill, W. A. Lahoz and A. C. Massacand, 2004: Sensitivity of tropospheric forecasts
613 to stratospheric initial conditions. *Q. J. R. Meteorol. Soc.*, **130**, 1771–1792.

614

615 Charlton, A. J., A. O’Neill, P. Berrisford and W. A. Lahoz, 2005a: Can the dynamical impact of the
616 stratosphere on the troposphere be described by large-scale adjustment to the stratospheric PV
617 distribution? *Q. J. R. Meteorol. Soc.*, **131**, 525-543.

618

- 619 Charlton, A. J., A. O'Neill, W. A. Lahoz, A. C. Massacand, and P. Berrisford, 2005b: The impact of the
620 stratosphere on the troposphere during the southern hemisphere stratospheric sudden warming, September
621 2002. *Q. J. R. Meteorol. Soc.*, **131**, 2171–2188.
- 622
- 623 Charron, M., S. Polavarapu, M. Buehner, P. A. Vaillancourt, C. Charrette, M. Roch, J. Morneau, L.
624 Garand, J. M. Aparicio, S. MacPherson, S. Pellerin, J. St-James, and S. Heilliette, 2012: The stratospheric
625 extension of the Canadian operational deterministic medium range weather forecasting system and its
626 impact on tropospheric forecasts. *Monthly Weather Review*, **140**, 1924-1944. DOI: 10.1175/MWR-D-11-
627 00097.1
- 628
- 629 Cucurull, L., R. A. Anthes, and L.-L. Tsao, 2014: Radio Occultation Observations as Anchor
630 Observations in Numerical Weather Prediction Models and Associated Reduction of Bias Corrections in
631 Microwave and Infrared Satellite Observations. *J. Atmos. Oceanic Technol.*, **31**, 20–32.
632 doi: <http://dx.doi.org/10.1175/JTECH-D-13-00059.1>
- 633
- 634 Daley, R. 1991: Atmospheric Data Analysis. Cambridge University Press. 457pp.
- 635
- 636 Dee, D. P., and 35 co-authors, 2011: The ERA-Interim reanalysis: Configuration and performance of the
637 data assimilation system. *Quart. J. R. Meteorol. Soc.*, **137**, 553-597. DOI: 10.1002/qj.828.
- 638
- 639 Dee, D. P., and S. Uppala, 2009: Variational bias correction of satellite radiance data in the ERA-Interim
640 reanalysis. *Quart. J. Roy. Meteor. Soc.*, **135**, 1830-1841.
- 641
- 642 Derber, J. C. and W.-S. Wu, 1998: The Use of TOVS cloud-cleared radiances in the NCEP SSI analysis
643 system. *Monthly Weather Review*, **126**, 2287-2299.

644

645 Douville, H., 2009: Stratospheric polar vortex influence on Northern Hemisphere winter climate
646 variability. *Geophys. Res. Lett.*, **36**, L18703, doi:10.1029/2009GL039334.

647

648 Errera, Q., M. Fujiwara, C. Long and D. Jackson, 2015: Report from the 10th SPARC data assimilation
649 workshop and the 2014 SPARC Reanalysis Intercomparison Project (S-RIP) workshop in Washington
650 DC, USA. SPARC Newsletter 44. Available from <http://www.sparc-climate.org/publications/newsletter/>

651

652 Gerber, Edwin, P., Amy Butler, Natalia Calvo, Andrew Charlton-Perez, Marco Giorgetta, Elisa Manzini,
653 Judith Perlwitz, Lorenzo M. Polvani, Fabrizio Sassi, Adam A. Scaife, Tiffany A. Shaw, Seok-Woo Son,
654 and Shingo Watanabe, 2012: Assessing and Understanding the Impact of Stratospheric Dynamics and
655 Variability on the Earth System. *Bull. Amer. Meteor. Soc.*, **93**, 845–859.

656 doi: <http://dx.doi.org/10.1175/BAMS-D-11-00145.1>

657

658 Healy, S. B. and Thépaut, J.-N., 2006: Assimilation experiments with CHAMP GPS radio occultation
659 measurements. *Q.J.R. Meteorol. Soc.*, **132**: 605–623. doi: 10.1256/qj.04.182

660

661 M. I. Hegglin, D. A. Plummer, T. G. Shepherd, J. F. Scinocca, J. Anderson, L. Froidevaux, B. Funke, D.
662 Hurst, A. Rozanov, J. Urban, T. von Clarmann, K. A. Walker, H. J. Wang, S. Tegtmeier, K. Weigel.
663 2014: Vertical structure of stratospheric water vapour trends derived from merged satellite data. *Nature*
664 *Geoscience* 7,768–776. doi:10.1038/ngeo2236

665

666 Hines, C. O., 1997. Doppler spread parametrization of gravity-wave momentum deposition in the middle
667 atmosphere. Part 1: Basic formulation. *J. Atmos. Sol. Terr. Phys.*, **59**, 371-386.

668

669 Hoppel, K. W., Baker, N. L., Coy, L., Eckermann, S. D., McCormack, J. P., Nedoluha, G. E., and
670 Siskind, D. E.: Assimilation of stratospheric and mesospheric temperatures from MLS and SABER into a
671 global NWP model, *Atmos. Chem. Phys.*, **8**, 6103-6116, doi:10.5194/acp-8-6103-2008, 2008.
672

673 Hoppel, Karl W., Stephen D. Eckermann, Lawrence Coy, Gerald E. Nedoluha, Douglas R. Allen, Steven
674 D. Swadley, and Nancy L. Baker, 2013: Evaluation of SSMIS Upper Atmosphere Sounding Channels for
675 High-Altitude Data Assimilation. *Mon. Wea. Rev.*, **141**, 3314–3330. doi: [http://dx.doi.org/10.1175/MWR-](http://dx.doi.org/10.1175/MWR-D-13-00003.1)
676 [D-13-00003.1](http://dx.doi.org/10.1175/MWR-D-13-00003.1)
677

678 Kobayashi, S., Y. Ota, Y. Harada, A. Ebita, M. Moriya, H. Onoda, K. Onogi, H. Kamahori, C.
679 Kobayashi, H. Endo, K. Miyaoka, and K. Takahashi , 2015: The JRA-55 Reanalysis: General
680 Specifications and Basic Characteristics. *J. Meteor. Soc. Japan*, **93**(1), 5-48, doi:10.2151/jmsj.2015-001.
681

682 Koshyk, J.N., Boville, B.A., Hamilton, K., Manzini, E., Shibata, K. 1999: Kinetic energy spectrum of
683 horizontal motions in middle-atmosphere models. *J. Geophys. Res.* **104**: 27177–27190.
684

685 Leovy, C., 1964: Simple models of thermally driven mesospheric circulation. *J. Atmos. Sci.*, **21**, 327-341.
686

687 Lei, L., Stauffer, D.R., Deng, A., 2012: A hybrid nudging-ensemble Kalman filter approach to data
688 assimilation. Part II: Application in a shallow-water model. *Tellus*, A 64 (1), 18485
689

690 Li, F., J. Austin, and J. Wilson, 2008: The strength of the Brewer–Dobson circulation in a changing
691 climate: Coupled chemistry–climate model simulations. *J. Climate*, **21**, 40–57.
692

- 693 Lindzen, R. S., 1981: Turbulence and stress owing to gravity wave and tidal breakdown. *J. Geophys. Res.*,
694 **86**, 9707-9714.
695
- 696 Lorenc, A. C., N. E. Bowler, A. M. Clayton, S. R. Pring, and D. Fairbairn, 2015: Comparison of Hybrid-
697 4DEnVar and Hybrid-4DVar Data Assimilation Methods for Global NWP. *Mon. Wea. Rev.*, **143**, 212–
698 229. doi: <http://dx.doi.org/10.1175/MWR-D-14-00195.1>
699
- 700 Lübken, F., M. Rapp, and P. Hoffmann, 2002: Neutral air turbulence and temperatures in the vicinity of
701 polar mesosphere summer echoes, *J. Geophys. Res.*, **107**(D15), 4273, doi:10.1029/2001JD000915.
702
- 703 Marshall, A. G., and A. A. Scaife. 2009: Impact of the QBO on surface winter climate, *J. Geophys. Res.*,
704 **114**, D18110, doi:10.1029/2009JD011737.
705
- 706 McLandress, C., 1998: On the importance of gravity waves in the middle atmosphere and their
707 parameterization in general circulation models. *Journal of Atmospheric and Solar-Terrestrial Physics*,
708 **60**, 1357-1383.
709
- 710 McLandress, C. and T. G. Shepherd, 2009: Simulated Anthropogenic Changes in the Brewer–Dobson
711 Circulation, Including Its Extension to High Latitudes. *J. Climate*, **22**, 1516–1540. doi:
712 <http://dx.doi.org/10.1175/2008JCLI2679.1>
713
- 714 McLandress, C., Shepherd, T. G., Polavarapu, S., and Beagley, S. R., 2012: Is missing orographic gravity
715 wave drag near 60° S the cause of the stratospheric zonal wind biases in chemistry-climate models?. *J.*
716 *Atmos. Sci.*, **69**, 802-818.
717

718 McLandress, C., J. F. Scinocca, T. G. Shepherd, M. C. Reader, and G. L. Manney, 2013: Dynamical
719 Control of the Mesosphere by Orographic and Nonorographic Gravity Wave Drag during the Extended
720 Northern Winters of 2006 and 2009. *J. Atmos. Sci.*, **70**, 2152–2169. doi: [http://dx.doi.org/10.1175/JAS-D-](http://dx.doi.org/10.1175/JAS-D-12-0297.1)
721 [12-0297.1](http://dx.doi.org/10.1175/JAS-D-12-0297.1)
722

723 McLandress, C., Plummer, D. A., and Shepherd, T. G.: Technical Note: A simple procedure for removing
724 temporal discontinuities in ERA-Interim upper stratospheric temperatures for use in nudged chemistry-
725 climate model simulations, *Atmos. Chem. Phys.*, **14**, 1547-1555, doi:10.5194/acp-14-1547-2014, 2014.
726

727 McNally, T., 2004: The assimilation of stratospheric satellite data at ECMWF. Proceedings of the
728 ECMWF/SPARC Workshop on Modelling and Assimilation for the Stratosphere and Tropopause, 23-26
729 June 2003. Available online from <http://www.ecmwf.int/publications/library/do/references/list/17123> .
730

731 Monge-Sanz, B. M., M. P. Chipperfield, D. P. Dee, A. J. Simmons and S. M. Uppala, 2013:
732 Improvements in the stratospheric transport achieved by a chemistry transport model with ECMWF
733 (re)analyses: identifying effects and remaining challenges. *Q. J. R. Meteorol. Soc.* **139**, 654–673.
734

735 Nezlin, Y., Y. J. Rochon and S. Polavarapu, 2009: Impact of tropospheric and stratospheric data
736 assimilation on mesospheric prediction. *Tellus*, **61A**(1), 154-159.
737

738 Ngan, K., G. E. Eperon, 2012: Middle atmosphere predictability in a numerical weather prediction
739 model: Revisiting the inverse error cascade. *Q. J. R. Meteorol. Soc.* **138**: 1366–1378. DOI:10.1002/qj.984
740

- 741 Orr, A., P. Bechtold, J. Scinocca, M. Ern, M. Janiskova, 2010: Improved Middle Atmosphere Climate and
742 Forecasts in the ECMWF Model through a Nonorographic Gravity Wave Drag Parameterization. *J.*
743 *Climate*, **23**, 5905–5926. doi: 10.1175/2010JCLI3490.1
744
- 745 Polavarapu, S. M., T. G. Shepherd, S. Ren and Y. J. Rochon, 2005: Some challenges of middle
746 atmosphere data assimilation. *Quart. J. Roy. Meteor. Soc.*, **131**, 3513-3527.
747
- 748 Pulido M. and J. Thuburn, 2005: Gravity wave drag estimation from global analyses using variational
749 data assimilation principles. I: Theory and implementation. *Q. J. Roy. Meteorol. Soc.*, **131**, 1821-1840.
750
- 751 Pulido M. and J. Thuburn, 2006: Gravity wave drag estimation from global analyses using variational
752 data assimilation principles. II: A case study. *Q. J. Roy. Meteorol. Soc.* **132**, 1527-1543.
753
- 754 Pulido M. and J. Thuburn, 2008: The seasonal cycle of gravity wave drag in the middle atmosphere. *J.*
755 *Climate*, **21**, 4664-4679.
756
- 757 Pulido M., S. Polavarapu, T. Shepherd and J. Thuburn, 2012: Estimation of optimal gravity wave
758 parameters for climate models using data assimilation. *Q. J. Roy. Meteorol. Soc.*, **138**, 298-309. DOI:
759 10.1002/qj.932.
760
- 761 Pulido, M, 2014: A Simple Technique to Infer the Missing Gravity Wave Drag in the Middle Atmosphere
762 Using a General Circulation Model: Potential Vorticity Budget. *J. Atmos. Sci.*, **71**, 683-696.
763
- 764 Ren, S., S. Polavarapu, T. G. Shepherd, 2008: Vertical propagation of information in a middle atmosphere
765 data assimilation system by gravity-wave drag feedbacks. *Geophys. Res. Lett.*, **35** (6), L06804, DOI:
766 10.1029/2007GL032699.

767

768 Ren, S., S. Polavarapu, S. R. Beagley, Y. Nezhin and Y. J. Rochon, 2011: The impact of gravity wave
769 drag on mesospheric analyses of the 2006 stratospheric major warming. *J. Geophys. Res.*, **116**, D19116,
770 doi:10.1029/2011JD015943

771

772 Rienecker, M.M., Suarez M.J., Gelaro R., Todling R., Bacmeister J., Liu E., and Coauthors. 2011,
773 MERRA: NASA's Modern-Era Retrospective Analysis for Research and Applications., *J. Climate*, **24**,
774 3624-3648

775

776 Ruiz J., M. Pulido and T. Miyoshi, 2013: Estimating parameters with ensemble-based data assimilation.
777 A review. *J. Meteorol. Soc. Japan*. **91**, 79-99.

778

779 Ruiz J. and M. Pulido, 2015: Parameter Estimation Using Ensemble Based Data Assimilation in the
780 Presence of Model Error. *Mon. Wea. Rev.* **143**, 1568–1582. DOI 10.1175/MWR-D-14-00017.1

781

782 Sandu, A. and T. Chai, 2011: Chemical data assimilation—An Overview. *Atmosphere*, **2**, 426-463.
783 doi:10.3390/atmos2030426

784

785 Sankey, D., S. Ren, S. Polavarapu, Y. J. Rochon, Y. Nezhin, S. Beagley, 2007: Impact of data assimilation
786 filtering methods on the mesosphere. *J. Geophys. Res.*, **D112** (24), D24104, doi:10.1029/2007JD008885.

787

788 Santitissadeekorn N. and C. Jones 2015: Two-stage filtering for joint state-parameter estimation. *Monthly*
789 *Weather Review*, **143**, 2028-2042.

790

- 791 Scinocca, J. F., 2003: An accurate spectral non-orographic gravity wave drag parameterization for general
792 circulation models. *J. Atmos. Sci.*, **60**, 667-682.
793
- 794 Scinocca, J.F., N.A McFarlane, M. Lazare, J. Li (2008), The CCCma Third Generation AGCM and its
795 Extension into the Middle Atmosphere. *Atmospheric Chemistry and Physics*, **8**, 7055-7074.
796
- 797 Shaw, T. A. and T. G. Shepherd, 2008: Raising the roof. *Nature geoscience*, **1**:12-13.
798
- 799 Shepherd, T. G., 2000: The middle atmosphere. *Journal of Atmospheric and Solar-Terrestrial Physics*,
800 **62**, 1587-1601.
801
- 802 Shepherd, T. G., 2002: Issues in stratosphere-troposphere coupling. *Journal of the Meteorological*
803 *Society of Japan*, **80B**, 769-792.
804
- 805 Shepherd, T. G., 2007: Transport in the middle atmosphere. *Journal of the Meteorological Society of*
806 *Japan*, **85B**, 165-191.
807
- 808 Shepherd, T. G., K. Semeniuk, and J. N. Koshyk, 1996: Sponge layer feedbacks in middle-atmosphere
809 models, *J. Geophys. Res.*, **101**, 23,447– 23,464.
810
- 811 Shepherd, T. G., D. A. Plummer, J. F. Scinocca, M. I. Hegglin, V. E. Fioletov, M. C. Reader,
812 E. Remsberg, T. von Clarmann and H. J. Wang, 2014: Reconciliation of halogen-induced ozone loss with
813 the total-column ozone record. *Nature Geoscience*, **7**, 443-449. DOI: 10.1038/NGEO2155
814
- 815 Sigmond, M., J. Scinocca, V. V. Kharin and T. G. Shepherd, 2013: Enhanced seasonal forecast skill
816 following stratospheric sudden warmings. *Nature Geoscience*, **6**, 98-102. doi:10.1038/ngeo1698

817

818 Smith, A., 2004: Physics and chemistry of the mesopause region. *Journal of Atmospheric and Solar-*
819 *Terrestrial Physics*, **66**, 839-857.

820

821 Stockdale, T. N., F. Molteni, and L. Ferranti, 2015: Atmospheric initial conditions and the predictability
822 of the Arctic Oscillation, *Geophys. Res. Lett.*, **42**,1173–1179, doi:10.1002/2014GL062681.

823

824 Tandeo, P., Pulido, M. and Lott, F., 2015: Offline parameter estimation using EnKF and maximum
825 likelihood error covariance estimates: Application to a subgrid-scale orography parametrization. *Q.J.R.*
826 *Meteorol. Soc.*, **141**: 383–395. doi: 10.1002/qj.2357

827

828 Thompson, D. W. J. and J. M. Wallace, 2001: Regional climate impacts of the Northern Hemisphere
829 Annular Model, *Science*, **293**, 85, DOI: 10.1126/science.1058958

830

831 Tripathi, O. P., Baldwin, M., Charlton-Perez, A., Charron, M., Eckermann, S. D., Gerber, E., Harrison, R.
832 G., Jackson, D. R., Kim, B.-M., Kuroda, Y., Lang, A., Mahmood, S., Mizuta, R., Roff, G., Sigmond, M.
833 and Son, S.-W. 2014: The predictability of the extratropical stratosphere on monthly time-scales and its
834 impact on the skill of tropospheric forecasts. *Q.J.R. Meteorol. Soc.* doi: 10.1002/qj.2432

835

836 Vallis, G. K., 2006: *Atmospheric and Oceanic Fluid Dynamics*. Cambridge University Press, 745 pp.

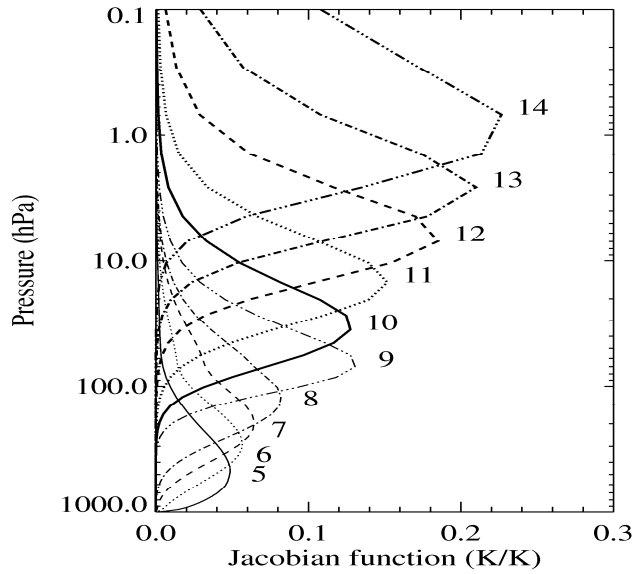
837

838 Wang, H., T. J. Fuller-Rowell, R. A. Akmaev, M. Hu, D. T. Kleist, and M. D. Iredell, 2011: First
839 simulations with a whole atmosphere data assimilation and forecast system: The January 2009 major
840 sudden stratospheric warming, *J. Geophys. Res.*, **116**, A12321, doi:10.1029/2011JA017081.

841

- 842 Watanabe S. 2008: Constraints on a Non-orographic Gravity Wave Drag Parameterization
843 Using a Gravity Wave Resolving General Circulation Model. *SOLA*, **4**, 61-64.
844
- 845 Xu, X., A. H. Manson, C. E. Meek, C. Jacobi, C. M. Hall, and J. R. Drummond (2011a), Mesospheric
846 wind semidiurnal tides within the Canadian Middle Atmosphere Model Data Assimilation System, *J.*
847 *Geophys. Res.*, **116**, D17102, doi:10.1029/2011JD015966.
848
- 849 Xu, X., A. H. Manson, C. E. Meek, C. Jacobi, C. M. Hall, and J. R. Drummond (2011b), Verification of
850 the mesospheric winds within the Canadian Middle Atmosphere Model Data Assimilation System using
851 radar measurements, *J. Geophys. Res.*, **116**, D16108, doi:10.1029/2011JD015589.

852



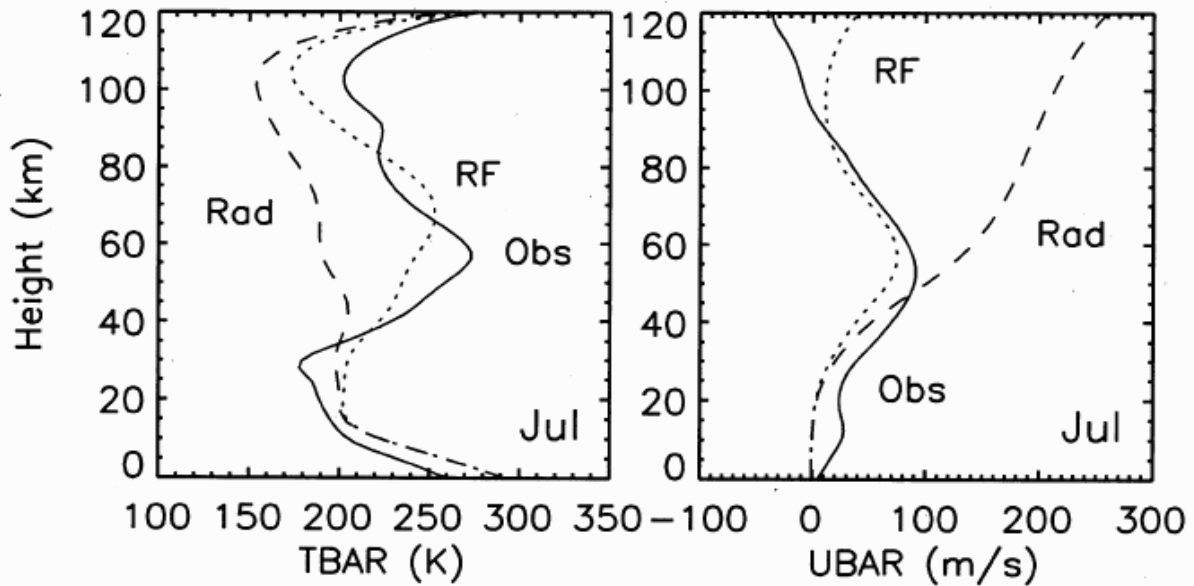
853

854

855 **Figure 1:** AMSU-A weighting functions on the 43 RTTOV levels computed using the US standard
856 atmosphere. Each function is identified by a channel number on the right. Only weighting functions for
857 channels 5 to 14 are shown. Figure courtesy of D. Shawn Turner.

858

859



860

861 **Figure 2:** Zonal mean temperature at 90 S (left) and zonal wind field at 40 S (right) during austral winter.

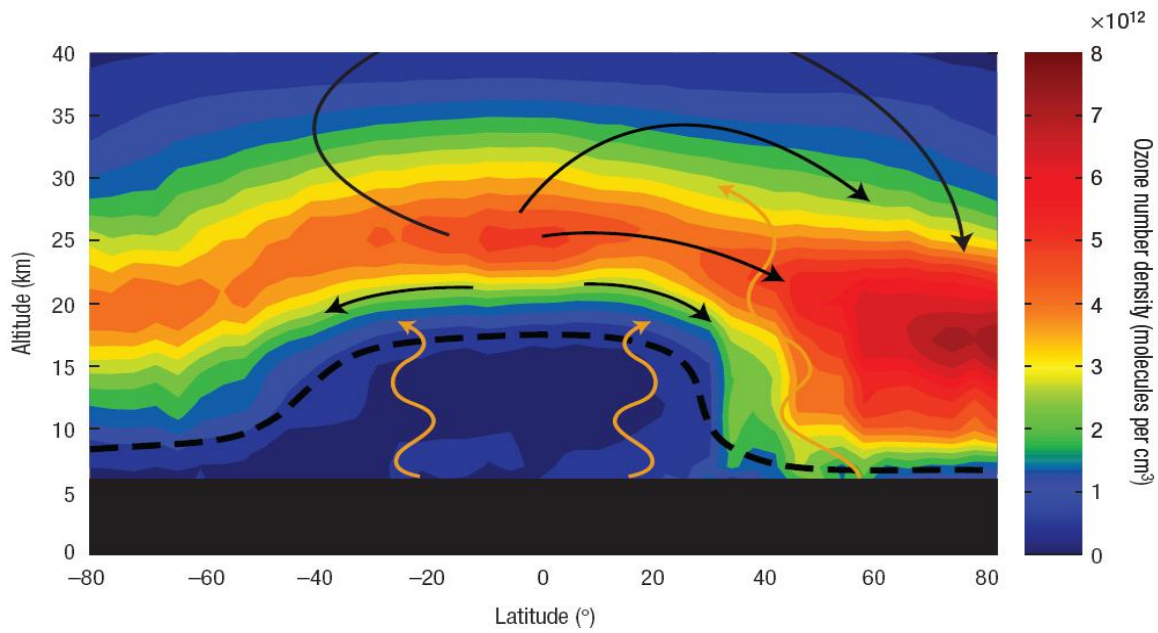
862 Observations from the COSPAR International Reference Atmosphere (CIRA) are shown as solid lines.

863 (COSPAR=COMmittee on SPAce Research). The profiles obtained from radiative equilibrium are shown

864 in dashed curves. Assuming a momentum force that is negative in the winter hemisphere and positive in

865 the summer hemisphere yields a better fit to observations (dotted curves). From McLandress (1998).

866

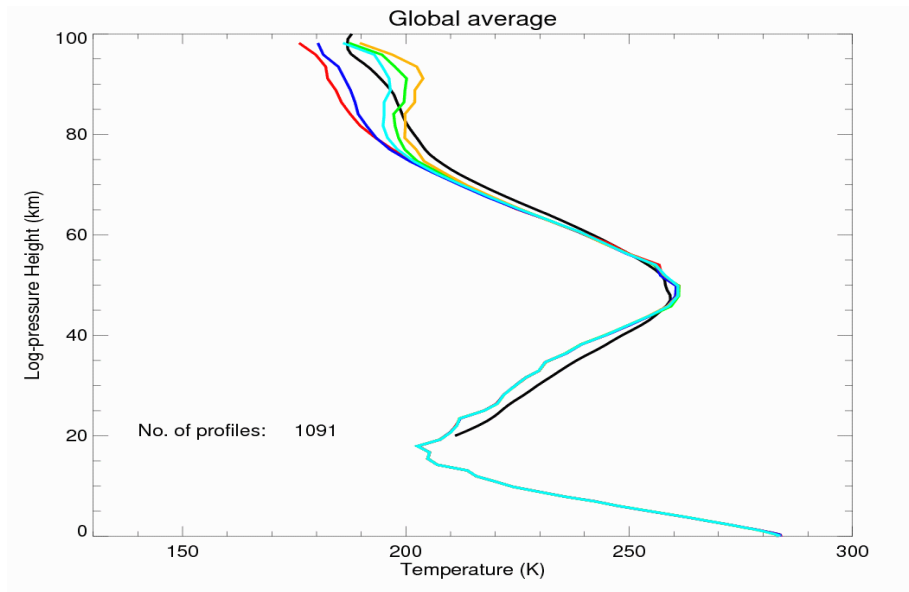


867

868 **Figure 3:** Cartoon of the Brewer-Dobson circulation. Meridonal circulation is indicated by black arrows.

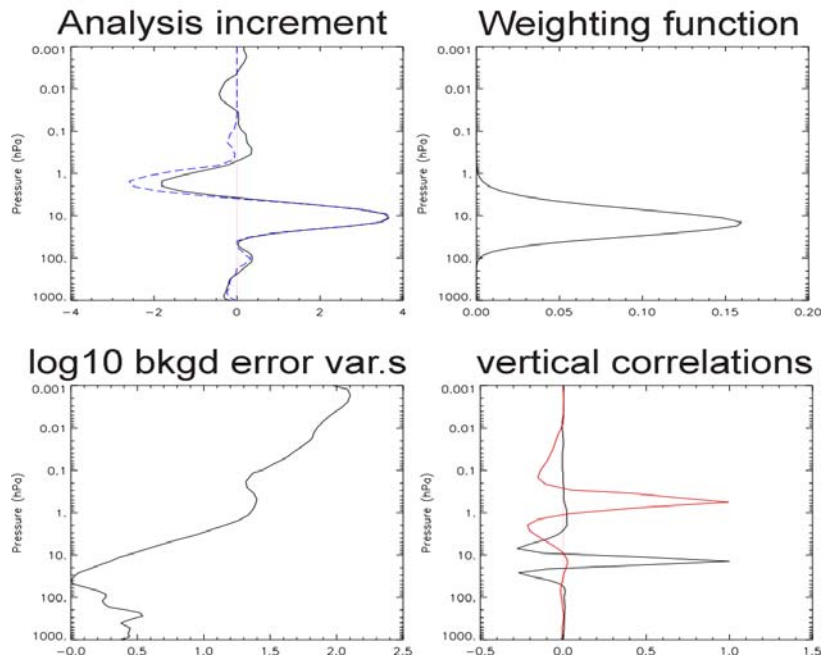
869 The tropopause is indicated by a heavy dashed line. The ozone distribution for March 2004 from OSIRIS

870 is shown in colours with values indicated by a colour bar on the right. From Shaw and Shepherd (2008).



871

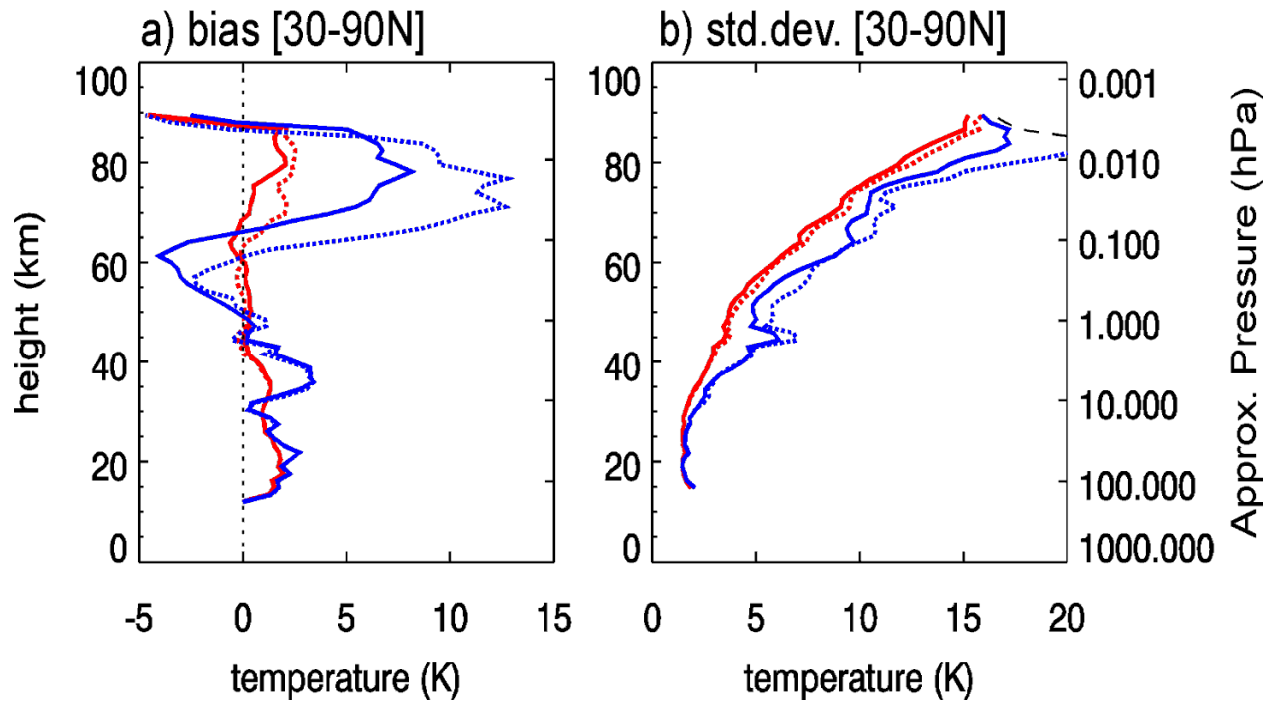
872 **Figure 4:** Average of CMAM-DAS temperature profiles sampled at SABER locations over the globe
 873 during 25 January 2002. The temperatures are from analyses obtained from assimilation experiments
 874 which were identical except for the externally applied filter. In all cases, observations were assimilated
 875 below 45 km only. The colours are black (SABER data), cyan (DF with 12-h cutoff), yellow (DF with 6-
 876 h cutoff), green (IAU with 6-h cutoff), blue (IAU with 4-h cutoff), and red (IAU with constant
 877 coefficients). Filter strength increases as follows: yellow-green-cyan-blue-red. From Sankey et al.
 878 (2007).



879

880

881 **Figure 5:** A 1-D assimilation of AMSU channel 11. Top left: Temperature analysis increments obtained
 882 when vertical correlations are unmodified (solid) or modified so that near zero values are exactly zero
 883 (dashed). Top right: weighting function for AMSU-A channel 11. Bottom left: log10 of temperature
 884 background error variance used with the CMAM-DAS. Bottom right: Two sample vertical correlation
 885 functions. From Polavarapu et al. (2005).



886

887

888 **Figure 6:** Fit of 6h temperature forecasts to SABER observations during 1-14 February 2006 using the
 889 CMAM data assimilation system. Assimilation cycles were run with parameterized gravity wave drag
 890 scheme (solid lines) or without it (dashed lines). Results from experiments in which SABER
 891 temperatures were assimilated are shown in red while those from experiments that did not assimilate
 892 those measurements are shown in blue. Panel (a) shows the bias from these 4 experiments while panel (b)
 893 shows the standard deviation for the northern hemisphere high latitudes. From Ren et al. (2011).